Nano Energy (2013) 2, 1197–1206

Available online at www.sciencedirect.com

ScienceDirect

journal homepage: www.elsevier.com/locate/nanoenergy

RAPID COMMUNICATION

Reactivation of dissolved polysulfides in Li-S batteries based on atomic layer deposition of Al_2O_3 in nanoporous carbon cloth

Xiaogang Han[a], Yunhua Xu[b], Xinyi Chen[a], Yu-Chen Chen[a], Nicholas Weadock[a], Jiayu Wan[a], Hongli Zhu[a], Yonglin Liu[a], Heqin Li[a], Gary Rubloff[a], Chunsheng Wang[b], Liangbing Hu[a,*]

[a]Department of Materials Science and Engineering, United States
[b]Department of Chemical Engineering, University of Maryland, College Park, Maryland 20742, United States

Received 9 March 2013; received in revised form 23 April 2013; accepted 6 May 2013
Available online 14 May 2013

KEYWORDS
Al_2O_3;
Atomic layer deposition;
Li-S battery;
Porous carbons;
Sulfur chemistry

Abstract
This work demonstrates the effect of atomic layer deposited (ALD) Al_2O_3 on the reactivation of dissolved polysulfides in Li-S batteries. A 0.5 nm thick layer of Al_2O_3 is conformally coated onto highly porous carbon cloth by ALD, and then assembled in a Li-S battery between the sulfur cathode and the anode side (separator and Li anode) to function as a reactivation component. Compared to half cells with no ALD treatment, the ultrathin Al_2O_3 coating increases the specific discharge capacity by 25% from 907 to 1136 mA h/g at the 1st cycle, and by 114% from 358 to 766 mA h/g at the 40th cycle. Thus the ALD-Al_2O_3 improves the initial specific capacity and stabilizes the cycle life remarkably. Scanning electron microscopy and energy-dispersive X-ray spectroscopy results indicate that the ALD-Al_2O_3 coated carbon cloth sorbs (adsorbs/absorbs) more dissolved sulfur species from the electrolyte. Potential mechanisms for the improved sorption properties are proposed. The combination of an ultrathin ALD-oxide coating with highly porous carbons presents a new strategy to improve the performance of Li-S batteries.

Introduction

Sulfur, an earth-abundant material, is one of the largest by-products of the petroleum industry [1,2]. As such, there is an emerging research field interested in finding novel applications of these sulfur wastes [3]. In the area of energy storage, sulfur has been intensely studied as a promising cathode material for lithium ion batteries (LIBs). Sulfur is a low cost, non-toxic material with a high theoretical specific energy density, 3-5 times higher than current intercalation chemistry-based LIBs [4]. These properties indicate a large potential market for sulfur as a cathode material in the near future [5]. Sulfur

*Corresponding author. Tel.: +1 301 405 9303; fax: +1 301 314 8514.
E-mail address: binghu@umd.edu (L. Hu).

2211-2855/$ - see front matter © 2013 Elsevier Ltd. All rights reserved.
http://dx.doi.org/10.1016/j.nanoen.2013.05.003

and lithium polysulfides (intermediates in Li-S batteries), however, are electronic insulators and high-order lithium polysulfides (Li_2S_x, $3 \leq x \leq 8$) readily dissolve in liquid electrolytes. Particularly, the dissolution-associated behaviors of the intermediate polysulfides reduce the amount of active sulfur available at the cathode. Also, the dissolved polysulfides transport through the electrolyte and dissipate energy at the lithium anode *via* direct chemical reactions, which triggers the so-called shuttle effect in Li-S batteries [6]. As a result, Li-S batteries suffer from low practical capacity and poor cycling stability [7]. Eliminating the sulfur dissolution problem is the primary challenge for future applications of Li-S batteries.

A lot of strategies in the area have been done to address the problem. Except for the passivation of lithium anodes with $LiNO_3$ [8-10] and alteration of electrolytes, [11-13] the majority of efforts have been devoted to engineering cathode composites. The most common tactic is to confine sulfur within various porous carbons, including mesoporous carbons, [14] microporous carbons[15], bimodal porous carbons,[16,17] hierarchical porous carbons, [18] hollow carbons, [19,20] carbon nanotube (CNT)/porous carbons, [21] and graphene/porous carbons [22]. Confinement within various conductive polymer/carbon matrices, such as PEDOT:PSS[23] and polyaniline [24] has also been explored. To further enhance the restriction of polysulfide dissolution, oxide nanoparticles ($Mg_{0.6}Ni_{0.4}O$, [7] Al_2O_3, [25] $Mg_{0.8}Cu_{0.2}O$ [26]) and porous oxide nanoparticles (SiO_2, [27] TiO_2 [28]) are added as sorption reagents of polysulfides. Another example is to restrict sulfur into polyacylonitrile structures for cathode composites [29]. All of these technologies were developed to confine the sulfur within the cathodes. The volume fluctuations in the discharge/charge process, however, inevitably affect the mechanical strength and morphology, [30] and thereby the validity of *in-situ* confinement.

Recently, the unique surface coating technique of atomic layer deposition (ALD) has gained attention for LIB fabrication [31]. Even on complicated 3-D nanostructures, ALD enables a conformal coating with precise thickness control at the atomic scale [32,33]. Most recently, the application of Al_2O_3 coatings on $LiCoO_2$, [34,35] $Li[Li_{0.20}Mn_{0.54}Ni_{0.13}Co_{0.13}]O_2$, [36] and natural graphite electrodes [37] by ALD greatly improved LIB cycling performance. It is suggested that the Al_2O_3 layer modifies electrolyte–electrode interface and prevents the active materials from dissolving.

In this work, we utilize an ALD-Al_2O_3 coating on porous carbon to solve the dissolution problem through a strategy of *ex-situ* collection (adsorption/absorption) and reactivation of the dissolved polysulfides in electrolyte. *Ex-situ* collection here refers to recovering the lost polysulfides from the electrolyte with a separate ALD layer, rather than confining sulfur species in an S-loading layer *in-situ*. Reactivation refers to the recovery of electrochemical activity of the collected sulfides given that the ultrathin ALD layer (<0.5 nm) is conductive. Fig. 1a illustrates a general configuration of Li-S batteries based on this strategy. Specifically, we employ a porous activated carbon cloth (ACC) as a basic reactivation layer. In the literature, nanosized Al_2O_3 particles have been shown to exhibit polysulfide adsorption in sulfur cathodes [25]. To enhance the sorption properties, a 0.5 nm thick ALD coating of Al_2O_3 is conformally deposited on the pore surfaces of the ACC fibers (Al_2O_3-ACC). The porous structure and the electrical conductivity of the ACC are expected to be maintained in the Al_2O_3-ACC samples, and the resulting Al_2O_3-ACC is expected to collect and reactivate more polysulfides than bare ACC under the same conditions (Fig. 1b). Recently, Nazar and co-workers utilized surface-initiated growth of thin oxide coatings directly onto modified mesoporous carbon-sulfur structures, [38] and Manthiram and Su inserted a CNT film interlayer to dramatically improve Li-S battery behavior [39,40]. The focus of our work is to understand how the combination of ultrathin ALD-Al_2O_3 with porous carbon improves Li-S battery performance.

Experimental section

Materials

Sulfur powder, bis(trifluoromethane)sulfonimide lithium salt (LiTFSI), and tetraethylene glycol dimethyl ether (TEGDME)

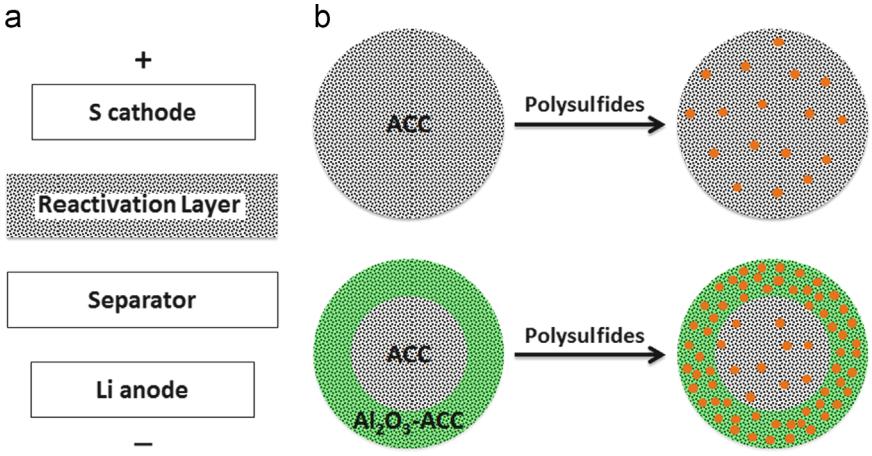

Figure 1 (a) Schematic of the Li-S battery with a conductive, porous carbon reactivation layer inserted between the sulfur cathode and separator. This reactivation layer functions to collect and reactivate the intermediate polysulfides (not shown) dissolved in electrolyte. (b) Illustrated cross-sections of ACC and ALD Al_2O_3 coated ACC (Al_2O_3-ACC) before and after collection of polysulfides in electrolyte. The ALD-Al_2O_3 coated ACC fiber maintains the highly porous structure and electrical conductivity while improving collection (adsorption/absorption) and reactivation of polysulfides.

were all purchased from Sigma-Aldrich. Active Carbon Cloth (ACC, Kynol™ 507-20) was provided free by Gun Ei Chemical Industry Co., Ltd. (Gunma, Japan). From the company data sheet, the ACC is 0.5 mm thick and has a specific surface area of 2000 m^2/g.

Infiltration of sulfur in ACC

The ACC was first punched into disks with a diameter of 1/4 in. (average 2.5 mg per piece). The ACC disks were hung on a platinum wire, and vacuum-sealed in a glass tube with sulfur powder. The samples were heated to 300 °C and hold for 6 h and cooled to room temperature for 24 h [41]. Typically the initial mass ratio of sulfur to ACC disks (20 pieces) in the glass tube was 1.5. Before and after heating, the mass of each disk was recorded with microbalance (Sartorius ME5, Data Weighing Systems, Inc.) to calculate the weight of infiltrated sulfur. The average sulfur loading per disk is 3.74 mg $\pm$ 0.27%, corresponding to 59 wt% or 12 mg/cm^2 of sulfur loading amount (Table S1 in supporting information).

Atomic layer deposition (ALD) of Al_2O_3 on ACC

The dry ACC disks (diameter: 1/4 in.) were placed into an atomic layer deposition system (Beneq TFS 500) for Al_2O_3 deposition. High-purity nitrogen at 150 °C was used as carrier gas for the whole process. To preserve the high conductivity of ACC as much as possible, only five cycles of ALD were performed. Each cycle includes alternating flows of trimethylaluminum (TMA, 4 s, Al precursor) and water (4 s, oxidant) separated by flows of pure nitrogen gas (4 and 10 s, respectively, carrier and cleaning gas). The thin layer of Al_2O_3 on ACC surfaces is estimated to be 0.5 nm according to a control of 200 cycles, 10 nm measured with atomic force microscopy (AFM).

Surface area and porosity tests for ACC and Al_2O_3-ACC

Nitrogen (N_2) adsorption and desorption isotherms were recorded with a Micromeritics ASAP 2020 Porosimeter Test Station. Samples of ACC and ALD Al_2O_3-ACC (0.5 g each) were used for the tests without any pre-treatment. The specific surface area was calculated by a single point at $P/P_0=0.3$, and the porosity distribution was calculated with the BJH (Barrett–Joyner–Halenda) equation.

I-V curve tests

ACC was cut into a 1×2 cm^2 rectangle and affixed to a glass slide for *I-V* testing. Silver glue adhered two 0.5 cm sections of the long side to the substrate, leaving a bare 1×1 cm^2. The sample was dried for 30 min at 60 °C to evaporate the solvents from the glue and form silver electrodes. The current-voltage (*I-V*) tests were performed at room temperature using a TT-prober manipulated probe system (Desert Cryogenics, LLC). The *I-V* properties of the Al_2O_3-ACC samples were tested in the same manner. Sheet resistances (Rs) of 90 and 170 Ω/sq. were calculated for ACC and Al_2O_3-ACC, respectively.

Assemblies of Li-S batteries with reactivation layers and electrochemistry tests

Two-electrode coin cells (CR2032) were assembled with lithium foil counter electrodes and 1 M LiTFSI in TEGDME electrolyte. The reactivation layer was inserted between the S-loading layer and the microporous membrane separator (Celgard 3501). The half cells were assembled in an argon-filled glovebox (oxygen content≤0.1 ppm, water content≤0.5 ppm). The half cells were charged and discharged between 1.0 and 3.0 V (*vs.* Li/Li^+) at room temperature (23–25 °C) using a BioLogic battery tester.

SEM and EDS characterizations

Scanning electron microscope (SEM) and energy-dispersive X-ray spectroscopy (EDS) characterizations were performed with a Hitachi SU-70 SEM. No conductive coatings were required to image the samples. The Al_2O_3-ACC reactivation layer samples removed from the Li-S cells were dip washed with TEGDME and acetone five times to remove any residual electrolyte. The cross-section samples were prepared by immersing the fibers in liquid nitrogen until frozen then fracturing them with clean tweezers.

Results and discussion

The Al_2O_3 coating is deposited by five cycles of ALD on an ACC disk (∅ 1/4 in.) at 150 °C under low pressure (2–3 mbar). The thickness of the ALD-Al_2O_3 coating layer is estimated to be no more than 0.5 nm (see Experimental section). For the sake of simplicity, the S-loading layer is also prepared with an ACC disk substrate by heating both sulfur powder and the disks together at 300 °C in a vacuum-sealed glass tube. The characteristic results of the as-prepared disks are shown in Fig. 2. Scanning electron microscopy (SEM) images reveal that the ACC fibers are smooth and straight with diameter of *ca.* 10 μm (Fig. 2a). The high magnification image in Fig. 2b highlights the highly porous surface. This morphology is favorable for ALD and sulfur-gas infiltration, as seen in elemental mapping of the cross-section of the samples (Fig. 2c–h).

Cross-section samples are obtained by fracturing the corresponding samples with clean tweezers in liquid nitrogen. Elemental mapping of the bare ACC (not displayed) reveals neither aluminum nor sulfur in the fibers. In addition to the uniformly distributed carbon (Fig. 2c,f), it is noted that trace amounts of oxygen from residual adsorbed water (O/C=0.02, atomic ratio) are present. For the S-loading layer (S-ACC), it is clear that sulfur distributes uniformly without aggregation (Fig. 2d,g). The Al_2O_3-ACC exhibits a well-defined annular pattern of elemental aluminum with minimal infiltration into the fiber (a dotted circle marks the boundary in Fig. 2h). The wall thickness of the annulet is about 2 μm (Fig. 2h and S1 in Supporting Information), and aluminum is uniformly distributed along the side walls of the Al_2O_3-ACC fibers (Fig. S2). Accordingly, it can be inferred

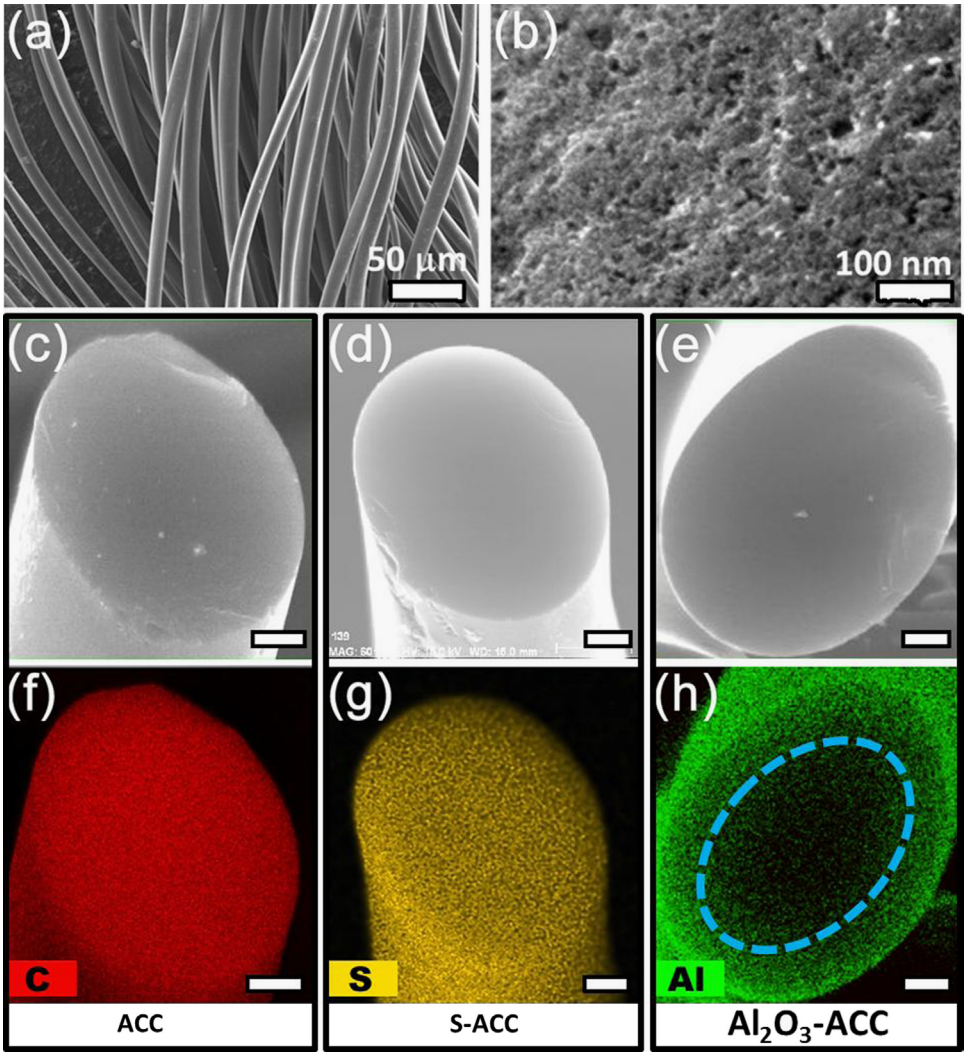

Figure 2 (a) and (b) SEM images of ACC fibers at different magnifications. (c)–(e) are SEM images and (f)–(h) are elemental maps from energy dispersive X-ray spectroscopy (SEM/EDS). (c) and (f) are for bare ACC, (d) and (g) are for ACC after sulfur loading (S-ACC), and (e) and (h) for ACC after ALD-Al_2O_3 (Al_2O_3-ACC). The dotted blue circle in (h) marks the boundary of major elemental aluminum distribution. All the scale bars in (c–h) are 2 μm.

that the Al_2O_3 is radially distributed along the entire fiber, consistent with the conformality of the ALD process.

The S-ACC and Al_2O_3-ACC are both fabricated with a solid-gas process at low pressures; however the penetration of sulfur is much greater than that of the Al_2O_3. This is a result of differences in the individual processes. The former is a continuous interaction of ACC with sulfur gas [42] for 6 h, followed by a 24-h cool down. The latter is a short, periodic reaction totaling less than 2 min for five cycles. As a result, sulfur has sufficient time to diffuse into and deposit uniformly within the porous fibers. In contrast, the Al_2O_3 precursors (water and trimethylaluminum) are only allowed a small diffusion time, forming the observed annular pattern.

Nitrogen adsorption and desorption isotherms are recorded to compare the surface area and porosity for the ACC and Al_2O_3-ACC samples. To preserve the Al_2O_3 coating layer on the ACC, the samples are not treated in the usual manner before characterization. As shown in Fig. 3a, both samples possess a coincident type-I isotherm, indicating microporous structures. The sample mass increase as a result of the 5-cycle ALD Al_2O_3 coating is negligible. The BET (Brunauer–Emmett–Teller) surface area is 1734 m^2/g for bare ACC and 1692 m^2/g for Al_2O_3-ACC, a 2.4% decrease. The value is close to that provided by the manufacturer (2000 m^2/g). A normalized porosity distribution is plotted in the Fig. 3a inset, and the calculated average pore diameter in ACC decreases from 2.6 to 2.4 nm with the 5-cycle ALD. The minimal decrease of the surface area and pore size in Al_2O_3-ACC confirms that the ALD coating does not block the ACC pores; maintaining the high surface area and porosity of the ACC. Enhanced sorption is likely for Al_2O_3-ACC considering the effect of Al_2O_3 nanoparticles on polysulfides [25].

The Al_2O_3-ACC disks need to be conductive to reactivate the sorbed sulfides and function as an extra current collector on the cathode side. Current–voltage (*I*–*V*) characteristics are measured for both Al_2O_3-ACC and bare ACC disks. As shown in Fig. 3b, the samples exhibit reversible ohmic curves between +0.5 and −0.5 V with two different slopes corresponding to the conductivity. The sheet

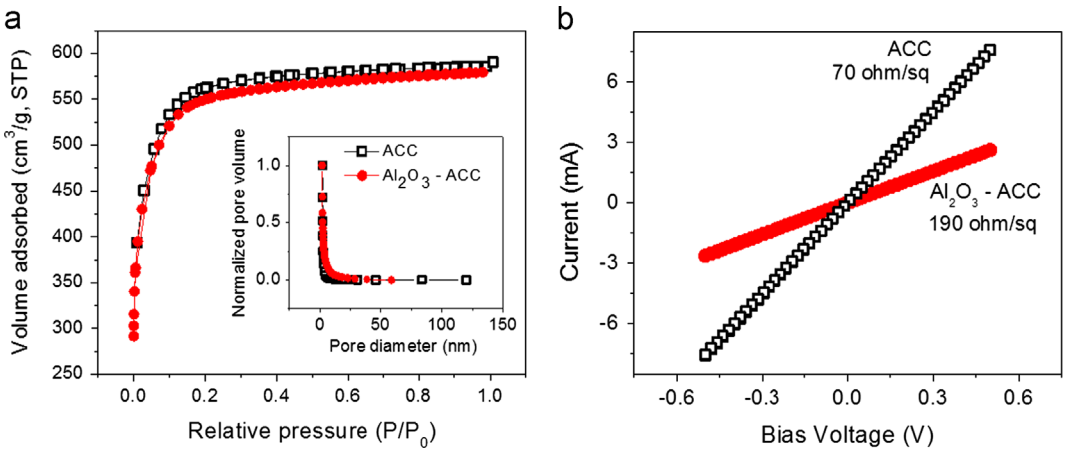

Figure 3 (a) Nitrogen adsorption/desorption isotherm and (inset) BJH (Barrett–Joyner–Halenda) pore-size distribution plot of ACC without (hollow squares) and with (solid circles) ALD-Al_2O_3 coating. (b) Current-voltage (*I*-*V*) profiles of ACC without and with ALD-Al_2O_3 coating.

resistances of the ACC and Al_2O_3-ACC samples are 70 Ω/sq. and 190 Ω/sq., respectively. Despite the increase in the sheet resistance, the Al_2O_3-ACC is still conductive enough for our application. To evaluate the collection/reactivation ability for the Al_2O_3-ACC experimentally, electrochemical tests are performed with battery devices according to Fig. 1. Coin cells are assembled using integrated an S-loading layer (S-ACC) and a collection/reactivation layer (ACC or Al_2O_3-ACC) as working electrode, and a lithium (Li) metal foil as counter electrode. Sulfur cathodes with only the S-ACC layer are characterized as a control. The S-ACC layers in all the three cathodes illustrated in Fig. 4 are ensured equal sulfur loading by preparation in the same batch (please see Fig. S3,S4 and Table S1,S2 for the detailed information).

Fig. 4 depicts the voltage profiles of the first two cycles for each battery. All three cathode configurations present typical features of the lithium-sulfur reaction; the specific capacities, however, are distinctly different. In Fig. 4a, the S-ACC control cathode exhibits an initial discharge capacity of 510 mA h/g, much less than the theoretical value. This capacity is less than the value reported for ACC as a binder-free cathode for Li–S batteries, [43] likely due to differences in the ACC types (conductivity and pore size). When a bare ACC reactivation layer is added, the initial capacity increases to 907 mA h/g (Fig. 4b). This trend is consistent with that reported by Manthiram and Su [39,40] using a CNT film as an interlayer in Li–S batteries. To estimate the capacity contribution of the ACC itself, ACC is tested as a sulfur-free cathode at the same conditions. The results display typical supercapacitor profiles with a discharge capacity of 55 mA h/g *vs.* ACC (Fig. S5). From the average weight ratio of ACC:S (5:3.75) in the test batteries (Fig. 4b), the contribution from ACC is 73 mA h/g *vs.* S, indicating the ACC contributes little to the capacity of the tested Li–S batteries. A rational explanation for the capacity increase with the ACC reactivation layer (S-ACC|ACC) is that the polysulfides dissolved in the electrolyte are adsorbed and reactivated on the neighboring ACC, recovering the lost capacity. Based on this hypothesis, replacing the bare ACC with an Al_2O_3-ACC reactivation layer (S-ACC|Al_2O_3-ACC, Fig. 4c) is expected to further improve the battery performance. The discharge capacity in Fig. 4c improves to 1136 mA h/g, consistent with our prediction. We conducted several batches of the tests, and all the results showed a similar specific capacity trend and ALD-Al_2O_3 treated reactivation layer exhibited a notable promotion for the cyclability. In Fig. 4a we note that the charge capacities are smaller than the corresponding discharge capacities. Quite a few sulfur species dissolved during the discharge process do not return to the cathode and become electrochemical inactive [44,45]. So the formation and dissolution of polysulfides leads to $Q_{charge} < Q_{discharge}$ in the initail discharge/charge cycles. The reactivation layer effectively re-collects and reactivates the dissolved polysulfides in liquid electrolyte, resulting in more equivalent charge and discharge capacities (Fig. 4b,c).

The batteries are cycled at room temperature, and discharge capacity *vs.* cycle number is plotted in Fig. 5. As anticipated, the capacity of the S-ACC cathode without the reactivation layer drops rapidly to 220 mA h/g after 10 cycles. The use of bare ACC as a reactivation layer increases the initial capacity, but a capacity of only 358 mA h/g (40% of the initial capacity) is retained after 40 cycles. In contrast, the ALD-Al_2O_3 coating improves both the cycling stability and capacity, and the capacity after 40 cycles is 766 mA h/g, 70% of the initial capacity. Comparing to the bare ACC reactivation layer, the presence of a 0.5 nm Al_2O_3 coating increases the specific discharge capacity by 25% at the 1st cycle, and by 114% at the 40th cycle. We intentionally set a low current density of 40 mA/g to increase polysulfide dissolution; however similar cycling behavior is observed at higher current densities. The gradual capacity fading of the batteries with the Al_2O_3-ACC reactivation layer may be due to the low fiber weave density of the ACC. Bundles of ACC fibers are separated by several hundred micrometers (Fig. S6), allowing a considerable amount of polysulfides to diffuse through the gaps without interacting with the reactivation layer. We predict that using a dense porous carbon film, *e.g.* carbonized electrospun fabric with an ALD-Al_2O_3 coating (Fig. S7) will improve reactivation further.

The cycling performance implies that the Al_2O_3-ACC reactivation layer captures more polysulfides than the bare

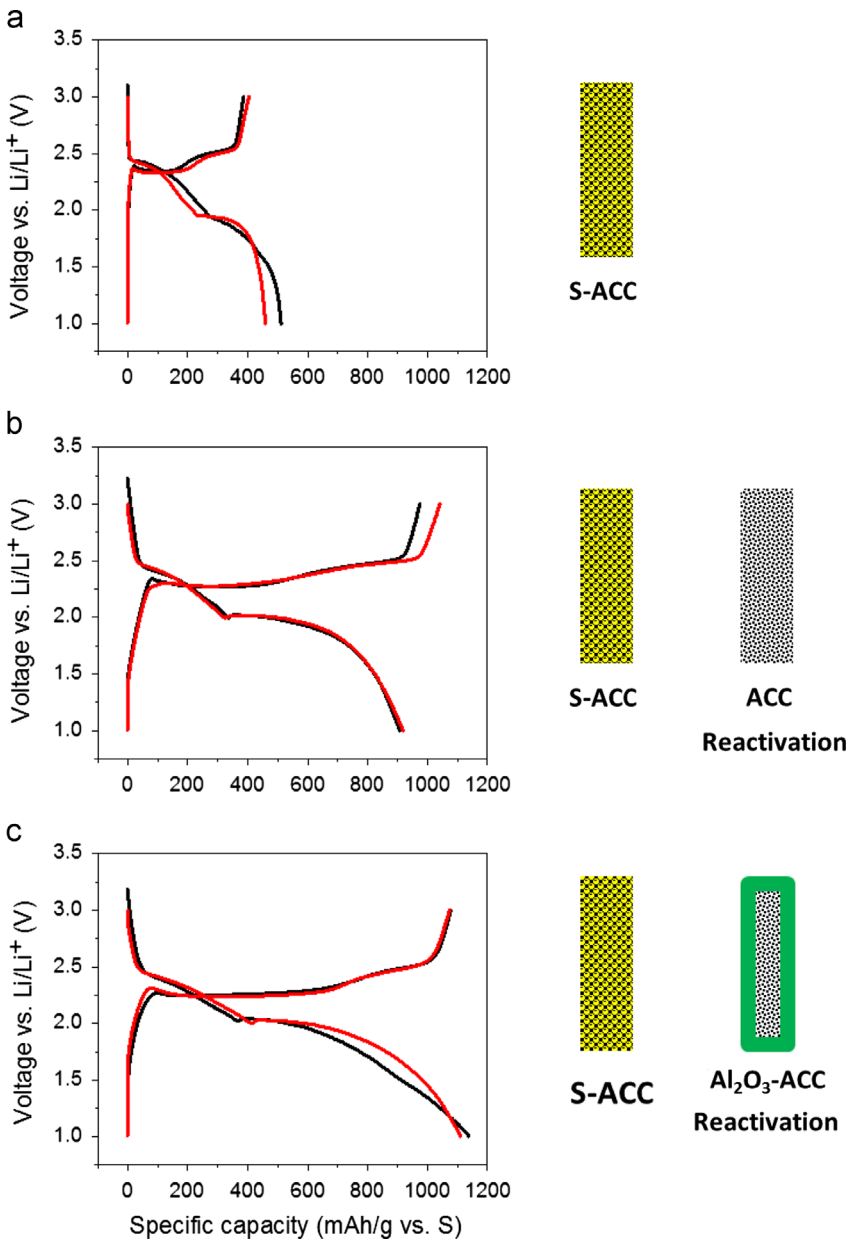

Figure 4 Comparison of the galvanostatic discharge/charge profiles of the first (black) and second (red) cycle of the Li-S batteries without a reactivation layer (a), with an ACC reactivation layer (b), and an Al_2O_3-ACC reactivation layer (c). The drawings next to the figures illustrate the corresponding cathode configurations.

ACC reactivation layer. To confirm this we examine EDS element maps of both reactivation layers immediately after cycling to fully charged states. The Li-S cells are disassembled and the layers washed five times with the solvent TEGDME and then acetone to remove any residual electrolyte. The cleaned reactivation layers are found to maintain their shapes, flexibility, and strength. Fig. 6a-c is the SEM micrographs for aluminum and sulfur distributions on the cross-section of a representative Al_2O_3-ACC fiber. Fig. 6b reveals that the aluminum distribution does not change during cycling, indicating the stable coating of ALD-Al_2O_3 on ACC. Most importantly, Fig. 6c displays that sulfur forms a distinguishable annulet with a 2 μm wall thickness (the boundary is marked with a dotted circle), coincident with

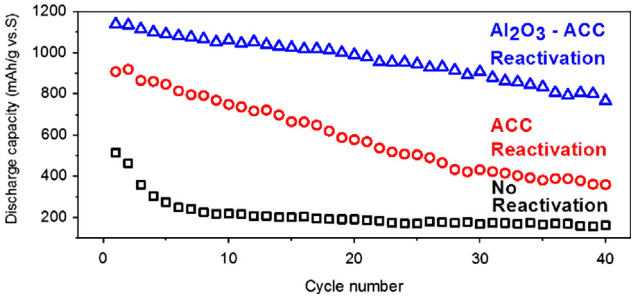

Figure 5 Discharge specific capacity *vs.* cycle number for Li-S batteries with cathode configurations as shown in Figure 4a, b and c.

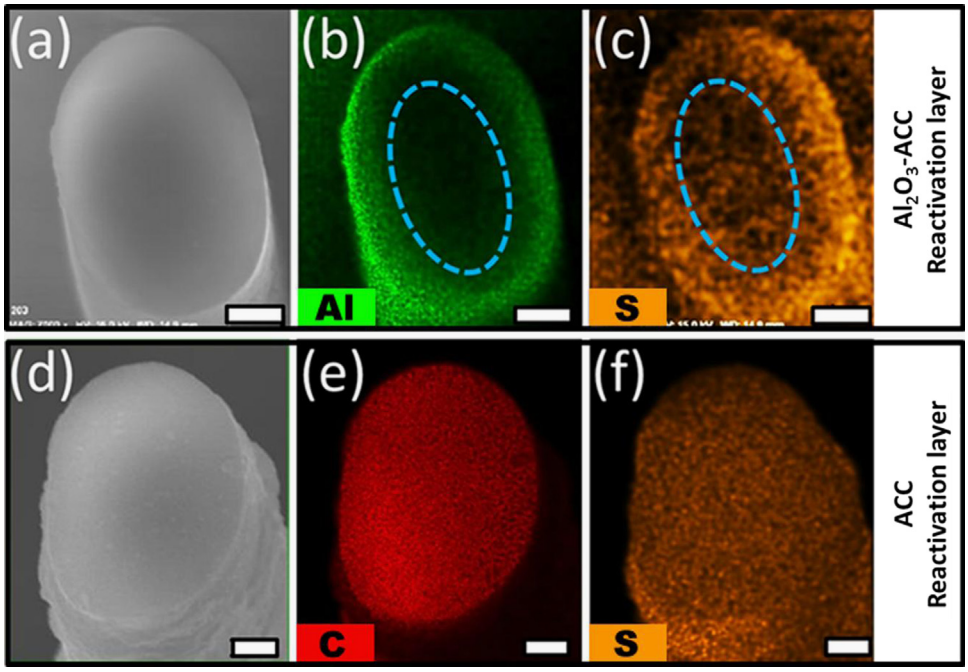

Fig. 6 SEM/EDS elemental mapping for Al_2O_3-ACC (a–c) and bare ACC (d–f) reactivation layers removed from Li–S batteries after cycling almost same time to fully changed states. (b,c) and (e,f) are elemental maps of Al, S, and C, S for the corresponding samples. The dotted blue circles in (b,c) mark the boundaries of the elemental Al and S annulet patterns. The brightness of the EDS patterns indicates the elemental intensities in the same image, but does not indicate the intensities in different images. All the scale bars are 2 μm.

the Al_2O_3 distribution in the fiber. The low density of sulfur interspersed in the fiber center is a result of sulfur diffusion. The annular Al_2O_3 region sorbs more sulfur species than the carbon center, directly confirming the stronger interaction of polysulfides with Al_2O_3 than with carbon.

Fig. 6d–f is element maps of the bare ACC reactivation layer. The sulfur distributes uniformly throughout the whole cross-section of the ACC carbon fiber. Comparison of the EDS data indicates that the Al_2O_3-ACC layer has a higher atomic ratio of sulfur to carbon (S/C=0.09) than the bare ACC layer (S/C=0.03), verifying that Al_2O_3-ACC layer effectively captures more polysulfides than bare ACC.

The coincident distribution of sulfur and aluminum in the Al_2O_3-ACC reactivation layers proves that the 5-cycle ALD process does not close the ACC pores and significantly retards polysulfide diffusion. Fig. 6f illustrates that the polysulfides are able to diffuse throughout the entire fiber during the cycling period. Hence, the sulfur-collection pattern in the Al_2O_3-ACC reactivation layer forms due to the interaction of sulfides with Al_2O_3, rather than insufficient diffusion time. The exact interaction between polysulfides and Al_2O_3 has not been determined; a potential mechanism involves chemisorption of the polysulfide species. Cyano-groups in PAN (polyacylonitrile) were recently suggested to attract polysulfides through the interaction with Li^+ [46]. It is reasonable that the lone pair electrons of oxygen groups in Al_2O_3 coordinate with lithium cations, and electrostatically attract polysulfide anions during the discharge/charge process. Another possible mechanism for the enhanced sorption in our system relates to the pore size. The average pore size of our Al_2O_3-ACC layer is 2.4 nm. This is closer to the length of typical polysulfide chains (<2 nm) [40] than bare ACC (2.6 nm), more favorable for sorption to polysulfides within the pores. In addition, the hydrophilicity and polarity of the ALD layer increases the wettability with respect to the liquid electrolyte, improving the electrochemical properties. Any of these properties of the ALD coating could facilitate the observed improvement of Li–S battery performance.

Conclusion

We have shown the viability of ultrathin ALD-Al_2O_3 for enhancing the collection (adsorption/absorption) and reactivation of dissolved polysulfides on ACC, improving the initial capacity and stabilizing the cycle life remarkably for Li–S batteries. We demonstrate this effect with a single ACC layer; other porous carbon films are possible substrates for the ALD-enhanced reactivation. Ultrathin ALD coatings maintain the high surface area of highly porous structures as well as the electrical conductivity of substrate. At the same time the ALD-oxide endows the surfaces with facilitated sorption of polysulfides due to the introduced chemisorption and decreased pore sizes. In addition, ALD coatings have several advantages for electrode engineering including conformal deposition, excellent stability, improved wettability, and minimal mass gain. To our knowledge, this is the first application of ALD for Li–S battery improvement, and it is expected to open a new direction for sulfur battery research.

Acknowledgments

This work has been supported by the Energy Frontier Research Center (EFRC) funded by the U.S. Department of Energy, Office of Science, and Office of Basic Energy Sciences. L.H. acknowledges the startup support from the University of Maryland, and we acknowledge the support of the Maryland NanoCenter and its FabLab and NispLab. The NispLab is supported in part by the NSF as a MRSEC shared experimental facility. X.H. and L.H. thank Dr. Wenzhong Bao for assistance in measuring *I*–*V* curves, Prof. Juchen Guo for the discussion on a possible mechanism, and Prof. Peter Kofinas for providing access to a high precision microbalance.

Appendix A. Supporting information

Supplementary data associated with this article can be found in the online version at http://dx.doi.org/10.1016/j.nanoen.2013.05.003.

References

[1] G. Kutney, Sulfur: History, Technology , Applications and IndustryChemTec. and its publisher is ChemTec Publishing, Toronto, Canada. It is 1 edition (January 15, 2007).
[2] U.S. Department of the Interior, Sulfur, Mineral Commodity Summaries, U.S. Geological Survey, 2012 publisher is U.S. Geological Survey, Reston, Virginia. Edited by U.S. Department of the interior (Ken Salazar, Secretary) and U.S. Geological Survey (Marcia K. McNutt, Director). The report pdf can be found on internet: http://minerals.usgs.gov/minerals/pubs/mcs/2012/mcs2012.pdf.
[3] W.J. Chung, A.G. Simmonds, J.J. Griebel, E.T. Kim, H.S. Suh, I.-B. Shim, R.S. Glass, D.A. Loy, P. Theato, Y.-E. Sung, K. Char, J. Pyun, Angewandte Chemie International Edition 50 (2011) 11409–11412.
[4] X. Ji, L.F. Nazar, Journal of Materials Chemistry 20 (2010) 9821–9826.
[5] P.G. Bruce, S.A. Freunberger, L.J. Hardwick, J.-M. Tarascon, Nature Materials 11 (2012) 19–29.
[6] C. Barchasz, J.-C. Lepretre, F. Alloin, S. Patoux, Journal of Power Sources 199 (2012) 322–330.
[7] M.S. Song, S.C. Han, H.S. Kim, J.H. Kim, K.T. Kim, Y.M. Kang, H.J. Ahn, S.X. Dou, J.Y. Lee, Journal of the Electrochemical Society 151 (2004) A791–A795.
[8] S.S. Zhang, J.A. Read, Journal of Power Sources 200 (2012) 77–82.
[9] D. Aurbach, E. Pollak, R. Elazari, G. Salitra, C.S. Kelley, J. Affinito, Journal of the Electrochemical Society 156 (2009) A694–A702.
[10] H.L. Wang, Y. Yang, Y.Y. Liang, J.T. Robinson, Y.G. Li, A. Jackson, Y. Cui, H.J. Dai, Nano Letters 11 (2011) 2644–2647.
[11] J. Gao, M.A. Lowe, Y. Kiya, H.D. Abruna, Journal of Physical Chemistry C 115 (2011) 25132–25137.
[12] D. Kumar, M. Suleman, S.A. Hashmi, Solid State Ionics 202 (2011) 45–53.
[13] A.S. Fisher, M.B. Khalid, M. Widstrom, P. Kofinas, Journal of the Electrochemical Society 159 (2012) A592–A597.
[14] J. Schuster, G. He, B. Mandlmeier, T. Yim, K.T. Lee, T. Bein, L.F. Nazar, Angewandte Chemie-International Edition 51 (2012) 3591–3595.
[15] F. Wu, S.X. Wu, R.J. Chen, S. Chen, G.Q. Wang, Chinese Chemical Letters 20 (2009) 1255–1258.
[16] D.-W. Wang, G. Zhou, F. Li, K.-H. Wu, G.Q. Lu, H.-M. Cheng, I.R. Gentle, Physical Chemistry Chemical Physics 14 (2012) 8703–8710.
[17] G. He, X. Ji, L. Nazar, Energy and Environmental Science 4 (2011) 2878–2883.
[18] S. Wei, H. Zhang, Y. Huang, W. Wang, Y. Xia, Z. Yu, Energy and Environmental Science 4 (2011) 736–740.
[19] G. Zheng, Y. Yang, J.J. Cha, S.S. Hong, Y. Cui, Nano Letters 11 (2011) 4462–4467.
[20] N. Jayaprakash, J. Shen, S.S. Moganty, A. Corona, L.A. Archer, Angewandte Chemie-International Edition 50 (2011) 5904–5908.
[21] S. Xin, L. Gu, N.-H. Zhao, Y.-X. Yin, L.-J. Zhou, Y.-G. Guo, L.-J. Wan, Journal of the American Chemical Society 134 (2012) 18510–18513.
[22] L.C. Yin, J.L. Wang, F.J. Lin, J. Yang, Y. Nuli, Energy and Environmental Science 5 (2012) 6966–6972.
[23] Y. Yang, G.H. Yu, J.J. Cha, H. Wu, M. Vosgueritchian, Y. Yao, Z.A. Bao, Y. Cui, Acs Nano 5 (2011) 9187–9193.
[24] G.C. Li, G.R. Li, S.H. Ye, X.P. Gao, Advanced Energy Materials 2 (2012) 1238–1245.
[25] Y.J. Choi, B.S. Jung, D.J. Lee, J.H. Jeong, K.W. Kim, H.J. Ahn, K.K. Cho, H.B. Gu, Physica Scripta T129 (2007) 62–65.
[26] Y. Zhang, X.B. Wu, H. Feng, L.Z. Wang, A.Q. Zhang, T.C. Xia, H.C. Dong, International Journal of Hydrogen Energy 34 (2009) 1556–1559.
[27] X.L. Ji, S. Evers, R. Black, L.F. Nazar, Nature Communications (2011) http://dx.doi.org/10.1038/ncomms1293.
[28] S. Evers, T. Yim, L.F. Nazar, Journal of Physical Chemistry C 116 (2012) 19653–19658.
[29] J.L. Wang, J. Yang, C.R. Wan, K. Du, J.Y. Xie, N.X. Xu, Advanced Functional Materials 13 (2003) 487–492.
[30] X. He, J. Ren, L. Wang, W. Pu, C. Jiang, C. Wan, Journal of Power Sources 190 (2009) 154–156.
[31] X.B. Meng, X.Q. Yang, X.L. Sun, Advanced Materials 24 (2012) 3589–3615.
[32] X.Y. Chen, E. Pomerantseva, P. Banerjee, K. Gregorczyk, R. Ghodssi, G. Rubloff, Chemistry of Materials 24 (2012) 1255–1261.
[33] H.C.M. Knoops, M.E. Donders, M.C.M. van de Sanden, P.H.L. Notten, W.M.M. Kessels, Journal of Vacuum Science and Technology A (2012) http://dx.doi.org/10.1116/1111.3660699.
[34] I.D. Scott, Y.S. Jung, A.S. Cavanagh, Y.F. An, A.C. Dillon, S.M. George, S.H. Lee, Nano Letters 11 (2011) 414–418.
[35] Y.S. Jung, P. Lu, A.S. Cavanagh, C. Ban, G.-H. Kim, S.-H. Lee, S.M. George, S.J. Harris, A.C. Dillon, Advanced Energy Materials 2 (2012) 1–7.
[36] K. Leung, Y. Qi, K.R. Zavadil, Y.S. Jung, A.C. Dillon, A.S. Cavanagh, S.H. Lee, S.M. George, Journal of the American Chemical Society 133 (2011) 14741–14754.
[37] Y.S. Jung, A.S. Cavanagh, L.A. Riley, S.H. Kang, A.C. Dillon, M.D. Groner, S.M. George, S.H. Lee, Advanced Materials 22 (2010) 2172–2176.
[38] K.T. Lee, R. Black, T. Yim, X. Ji, L.F. Nazar, Advanced Energy Materials 2 (2012) 1490–1496.
[39] Y.-S. Su, A. Manthiram, Chemical communications (Cambridge, England) 48 (2012) 8817–8819.
[40] Y.-S. Su, A. Manthiram, Nature Communications 3 (2012), The reference is provided a article number 1166, and the page is 1-5. http://www.nature.com/ncomms/journal/v3/n10/full/ncomms2163.html.
[41] J.C. Guo, Y.H. Xu, C.S. Wang, Nano Letters 11 (2011) 4288–4294.
[42] A.G.M. Ferreira, L.Q. Lobo, Journal of Chemical Thermodynamics 43 (2011) 95–104.
[43] R. Elazari, G. Salitra, A. Garsuch, A. Panchenko, D. Aurbach, Advanced Materials 23 (2011) 5641–5644.
[44] J.L. Wang, J. Yang, J.Y. Xie, N.X. Xu, Y. Li, Electrochemistry Communications 4 (2002) 499–502.
[45] X. Liang, Z. Wen, Y. Liu, H. Zhang, L. Huang, J. Jin, Journal of Power Sources 196 (2011) 3655–3658.

[46] J. Guo, Z. Yang, Y. Yu, H.D. Abruña, L.A. Archer, Journal of the American Chemical Society 135 (2012) 763–767.

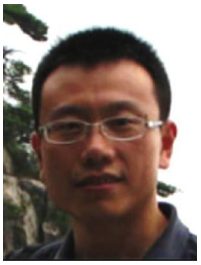

Xiaogang Han received his B.S. in material chemistry from Shanxi University in China in 2000. He obtained his Ph.D. in Analytical chemistry at the University of Science and Technology of China (USTC) in 2009. In this period, he studied on electrochemistry, DNA nanotechnology, and self-assembly of nanobjects with Prof. Zhaoxiang Deng. As a postdoc at University of California, Riverside from 2009 to 2011, he worked with Prof. Yadong Yin, and studied on various synthesis methods and applications of inorganic nanomaterials, including Pd, Au, Ag, SiO2, TiO2, ZnS, CdS, Fe2O3, etc. Currently, he is a research associate at University of Maryland, College Park. His research interests focus on energy storage, flexible electronics and ALD-based manufacturing.

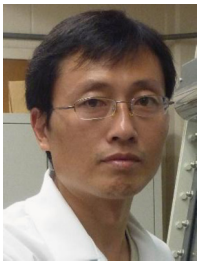

YunhuaXu received his Ph.D. degree in Materials Physics and Chemistry from South China University of Technology in 2008 and was a postdoctoral fellow in the Center for Polymers and Organic Solids at the University of California, Santa Barbara. He is currently an Assistant Research Scientist at the University of Maryland, College Park. His research interests focus on electrode materials and electrochemistry for rechargeable batteries, including Li-ion and Na-ion batteries.

Xinyi Chen just completed his PhD under supervision of Prof. Gary Rubloff in Materials Science and Engineering from University of Maryland, College Park. During his doctoral work, he was a Future Faculty Fellow and a receiver of Chinese Government Award for Outstanding Self-financed Students Abroad. He holds a Master and Bachelor degree in Physics from Nanjing University, China. He is now a R&D engineer with LAM Research. His research interest is in synthesis of thin films and nanomaterials with applications to electronics, energy storage and energy harvesting devices.

Yu-Chen Chen received a master degree in Materials Science and Engineering in University of Maryland, College Park, US and a bachelor degree in Mechanical Engineering in Chang Gung University, Taiwan. He also joined research group in Energy Research Center and NISP, NanoCenter in University of Maryland. His research interests are electron microscopy research and electro chemical energy storage devices.

Nicholas Weadock received his B.Sc. in Materials Science and Engineering from the University of Maryland, College Park, in 2013. He will pursue his Ph.D. in Materials Science at the California Institute of Technology. His current research involves nanomechanical studies of sodium ion batteries.

Jiayu Wan is currently a PhD candidate at University of Maryland, College Park. His research interests are mainly on nanomaterials and nanotechnology for energy storage and 2D materials based electronic devices (transparent electrode, transistors, sensors etc.) Jiayu obtained his BS degree in Huazhong University of Science and Technology in China in 2011.

Zhu is currently a research associate at the University of Maryland. Her work with Prof. Liangbing Hu focuses on transparent flexible electronic and energy storage. She received her PhD degree in Wood Chemistry and Paper Making Technology at South China University of Technology. From 2007 to 2008, Zhu conducted research in the Western Michigan University.Since 2009, she has worked at Nanjing Forestry University as an assistant professor. She conducted research on materials science and processing of degradable and renewable biomaterials from natural wood with Dr. Gunnar Henriksson at the Royal Institute of Technology in Sweden.

Yonglin Liu is currently a Patent Agent at Quarles & Brady LLP. He received his Ph.D. degree in Organic Chemistry from the Johns Hopkins University in 2006. He worked at National Institute of Standards and Technology (NIST) with a National Research Council (NRC) Research Associate fellowship and as a guest research scientist from 2006-2011. From 2011- 2012, Yonglin briefly worked as a research scientist at University of Maryland, College Park. Yonglin's research interest was including nanomaterials for energy and electronic applications. Yonglin has extensive experience in a broad range of technology fields including Medicinal Chemistry, Nanotechnology/Nanomaterials (production, application, etc.), Organic Chemistry, Inorganic Chemistry, Semiconductor, Biophysics, Life Science, Materials Science and Engineering, Energy (battery, capacitors, etc.), Lasers, Electrical Engineering, Mechanical Engineering, etc.

Dr. Heqin Li is a Professor in the department of Materials Science and Engineering at Hefei University of technology, China. She received her Ph.D. degree in the institute of Solid State Physics at Chinese Academy of Sciences. Her research interests are next generation of Li-ion battery, nanofabrication of semiconductor devices, and nano oxide film deposition.

Gary Rubloff is Minta Martin Professor of Engineering in the Department of Materials Science and Engineering and the Institute for Systems Research at the University of Maryland, where he is the founding director of both the Maryland NanoCenter and Nanostructures for Electrical Energy Storage (NEES), a DOE Energy Frontier Research Center. He is the recipient of the AVS Gaede-Langmuir Prize and Fellow of AVS and APS. His research is currently focused on nanostructures for energy, atomic layer deposition, and biofabricated microsystems.

Dr. Chunsheng Wangis an Associate Professor in the Chemical & Biomolecular Engineering at the University of Maryland. He received his Ph.D. from Zhejinag University, China in Materials Science and Engineering. Prior to joining University of Maryland in August, 2007, he was an assistant professor in Department of Chemical Engineering at Tennessee Technological University (TTU) in 2003-2007 and a Research Scientist in Center for Electrochemical System and Hydrogen Research at Teas A&M University in 1998-2003. His research focuses on Li-ion batteries and fuel cells.

Liangbing Hu received his B.S. in applied physics from the University of Science and Technology of China (USTC) in 2002. He did his Ph.D. in experimental physics at UCLA, focusing on carbon nanotube based nanoelectronics. In 2006, he joined UnidymInc (www.unidym.com) as a co-founding scientist, and his role was the development of roll-to-roll printed carbon nanotube trans parent electrodes and device integrations into touch screens, LCDs, flexible OLEDs and solar cells. As a postdoc at Stanford from 2009 to 2011, he worked on various energy devices including Li-ion batteries, ultracapacitors and microbial fuel cells. Currently, he is an assistant professor at University of Maryland College Park. His research interests include energy science and devices, flexible electronics and nanomanufacturing.